# Structural Properties of Opals Grown with Vertical Controlled Drying

Alex Hartsuiker*,† and Willem L. Vos†,‡

*FOM Institute for Atomic and Molecular Physics AMOLF, Kruislaan 407, 1098 SJ Amsterdam, The Netherlands, and Complex Photonic Systems, MESA+ Research Institute, University of Twente, The Netherlands*

*Received January 15, 2008*

We have grown thin opals of self-assembled silica colloids by the well-known vertically controlled drying method. The volume fraction at the start of the growth and the temperature were systematically varied. We have quantitatively characterized the lateral domain sizes by scanning electron microscopy. The sample thickness as a function of position was obtained from Fabry−Pérot fringes measured in optical reflectivity. We observe that the sample thickness strongly increases from top to bottom, independent of temperature, in agreement with a model that we propose. The inhomogeneity in thickness contrasts with earlier reports. The lateral domain shapes of the single-crystal domains are found to vary from irregular near the top to rectangular near the bottom. A surprising observation is that, grosso modo, the lateral domain extents increase linearly with thickness (i.e., thin crystals are small, and thick crystals are large). This behavior agrees qualitatively with results on completely different colloids such as disordered slurries. The consequence of our results for optical applications, including photonic crystals, is that unwanted scattering due to grain boundaries is reduced for large domains that are thick. Conversely, thin crystals will scatter relatively strongly from grain boundaries.

## I. Introduction

Monodisperse nanometer particles have the ability to self-assemble into colloidal photonic crystals. These self-assembled photonic crystals, also called artificial opals, have attracted much attention over the last few years. They have face-centered cubic packing and were used by many groups as a template to create so-called inverse opals.[1−4] Both silica and polystyrene nanospheres have been used to create templates for the synthesis of titania[1] and silicon[2,3] inverse opals for photonic crystal applications, respectively.

Methods such as sedimentation and vertically controlled drying,[5] among others,[6] have been introduced with respect to the formation of thick- and thin-film opals, respectively. In the sedimentation method, the spheres in a suspension are left to sediment naturally.[7,8] Spheres with radii larger than 400 nm do not have time to arrange themselves in crystalline packing because of sedimentation that is too fast,[9] leading to lower crystalline quality. A solution to this problem was proposed by Holgado et al., who used electrophoresis to slow down the spheres.[9] Control of the shape of the crystal remains limited by sedimentation; therefore, vertically controlled drying has become the most favorable method lately. This method is based on the one that Dimitrov and Nagayama used to deposit monolayers of submicrometer spheres onto a substrate.[10] The vertically controlled drying technique pioneerd by Jiang et al.[5] consists of placing a substrate into a dispersion. When the solvent evaporates, the spheres form a thin crystalline layer on the substrate.

A lot of work has been published on the vertically controlled drying method. Despite much work, there is still an ongoing debate about crystal formation,[10,11] and the size and thickness limits of crystal domains have not been investigated. These limits are the subject of this article. The thickness of the crystal determines the intensity and the relative line width of Bragg reflections,[12,13] and its limits are therefore relevant to optical applications. The lateral sizes of photonic crystals should be larger than the size of a typically used laser beam. Also, crystals should be large enough to allow functionalization with waveguides[14] and cavities.[15] Interestingly, the shape and size of the domains contain valuable information on the drying process.[16−22]

Crack formation during the infiltration of opals has been investigated.[23] It was shown qualitatively that the calcination of spheres increased the crystal domain size of the inverse photonic crystal after LPCVD infiltration at 550 °C.

* Corresponding author. E-mail: hartsuiker@amolf.nl. URL:www.photonicbandgaps.com.

† FOM Institute for Atomic and Molecular Physics AMOLF.

‡ University of Twente.

(1) Wijnhoven, J. E. G. J.; Vos, W. L. *Science* **1998**, *281*, 5378.
(2) Vlasov, Y. A.; Bo, X. Z.; Sturm, J. C.; Norris, D. J. *Nature* **2001**, *414*, 289.
(3) Blanco, A.; Chomski, E.; Grabtchak, S.; Ibisate, M.; John, S.; Leonard, S. W.; López, C.; Meseguer, F.; Míguez, H.; Mondia, J. P.; Ozin, A. O.; Toader, O.; van Driel, H. M. *Nature* **2000**, *405*, 437.
(4) Meseguer, F.; Blanco, A.; Míguez, H.; García-Santamaría, F.; Ibisate, M.; López, C. *Colloids Surf., A* **2002**, *202*, 281.
(5) Jiang, P.; Bertone, J. F.; Hwang, K. S.; Colvin, V. L. *Chem. Mater.* **1999**, *11*, 2132.
(6) Meseguer, F. *Colloids Surf., A* **2005**, *270*, 1.
(7) Vos, W. L.; Megens, M.; vanKats, C. M. *Langmuir* **1997**, *13*, 6004.
(8) Míguez, H.; Meseguer, F.; López, C.; Blanco, A.; Moya, J. S.; Requena, J.; Mifsud, A.; Fornes, V. *Adv. Mater.* **1998**, *10*, 480.
(9) Holgado, M.; García-Santamaría, F.; Blanco, A.; Ibisate, M.; Cintas, A.; Míguez, H.; Serna, S. J.; Molpeceres, C.; Requena, J.; Mifsud, A.; Meseguer, F.; López, C. *Langmuir* **1999**, *15*, 4701.
(10) Dimitrov, A. S.; Nagayama, K. *Langmuir* **1996**, *12*, 1303.
(11) Norris, D. J.; Arlinghaus, E. G.; Meng, L.; Heiny, R.; Scriven, L. E. *Adv. Mater.* **2004**, *16*, 1393.
(12) Galisteo Lòpez, J. F.; Vos, W. L. *Phys. Rev. E* **2002**, *66*, 036616.
(13) Bertone, J. F.; Hwang, K. S.; Mittleman, D. M.; Colvin, V. L. *Phys. Rev. Lett.* **1999**, *83*, 300.
(14) Braun, P. V.; Rinne, S. A.; García Santamaría, F. *Adv. Mater.* **2006**, *18*, 2665.
(15) Woldering, L. A.; Otter, A. M.; Husken, B. H.; Vos, W. L. *Nanotechnology* **2006**, *17*, 5717.
(16) Allain, C.; Lima, L. *Phys. Rev. Lett.* **1995**, *74*, 2981.
(17) Dufresne, E. R.; Corwin, E. I.; Greenblatt, N. A.; Ashmore, J.; Wang, D. Y.; Dinsmore, A. D.; Cheng, J. X.; Xie, X. S.; Hutchinson, J. W.; Weitz, D. A. *Phys. Rev. Lett.* **2003**, *91*, 224501.
(18) Shorlin, K. A.; de Bruyn, J. R.; Graham, M.; Morris, S. W. *Phys. Rev. E* **2000**, *61*, 6950.
(19) Li, H.; Marlow, F. *Chem. Mater.* **2005**, *17*, 3809.
(20) Dufresne, E. R.; Stark, D. J.; Greenblatt, N. A.; Cheng, J. X.; Hutchinson, J. W.; Mahadean, L.; Weitz, D. A. *Langmuir* **2006**, *22*, 7144.
(21) Li, H.; Marlow, F. *Chem. Mater.* **2006**, *18*, 1803.
(22) Singh, K. S.; Tirumkudulu, M. S. *Phys. Rev. Lett.* **2007**, *98*, 218302.
(23) Chabanov, A. A.; Jun, Y.; Norris, D. J. *Appl. Phys. Lett.* **2004**, *84*, 3573.

10.1021/la800137e CCC: $40.75 
Published on Web 03/27/2008

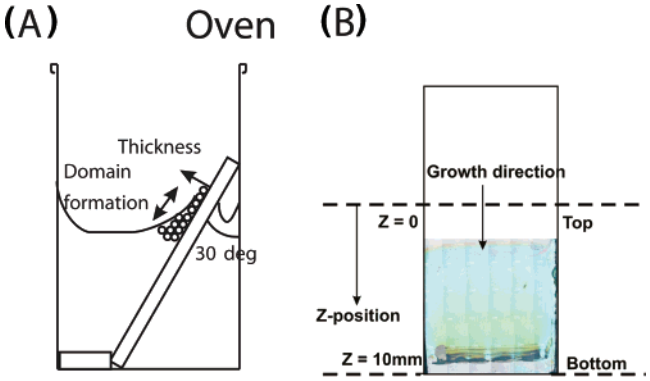


**Figure 1.** (A) Setup used for the growth of the thin film opals. The substrate is placed in a dispersion at an angle of 30°. The domains form in the direction parallel to the surface, and the thickness is defined perpendicular to the sample. (B) Optical microscope picture of a typical opal. The growth direction, the top, and the bottom are indicated. This terminology is also used in the text.

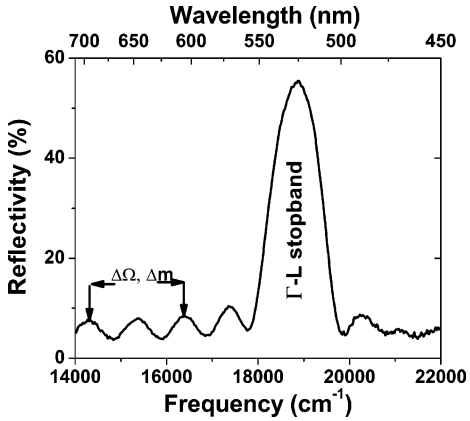


**Figure 2.** Reflectivity spectrum showing a first-order stopband and Fabry−Pérot fringes. The high reflectivity peak of 55% at 18 880 $cm^{-1}$ is the result of the $\Gamma - L$ stopband. The frequency difference between $\Delta m$ Fabry−Pérot fringes is indicated by $\Delta\Omega$. Here, $\Delta m = 2$ and $\Delta\Omega = 2083$ $cm^{-1}$ are indicated.

Here we have grown opal photonic crystals while varying the growth temperature and the volume fraction of the dispersion. We will focus on two structural parameters, namely, the domain size and the thickness of the crystal, to obtain a 3D picture of the crystal domains. We will discuss the limits of the vertically controlled drying technique with respect to crystal domain size and thickness.

## II. Experimental Section

**A. Opal Fabrication.** We used silicon dioxide colloidal spheres synthesized with a microemulsion method[24] and used earlier by Megens et al.[25] These spheres have a radius of 113 nm with a polydispersity of 1.5% and were dispersed in ethanol. The opals were grown with the vertically controlled drying method[5] on a 2.5-cm-long glass substrate and placed under at angle of 30° with respect to the vertical walls of the beaker (Figure 1B). The beaker with the substrate and 2 mL of solution was placed inside an oven. The temperature $T$ of the oven and the initial volume fraction of spheres in the dispersion ($\Phi_i$) were varied in the experiments discussed here. The accuracy of the volume fraction of the bulk is conservatively estimated to be within 5% of $\Phi_i$. The temperature $T$ is estimated to stay constant to within 1°. We chose temperatures to increase the evaporation speed of ethanol with respect to room temperature, but

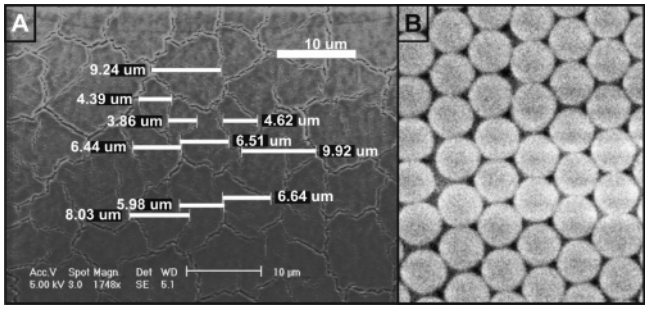


**Figure 3.** (A) Scanning electron microscope photograph of an artificial opal. The photograph shows single-crystal domains that are bounded by grain boundaries or cracks. The labels indicate the measured domain widths. The 10 values measured from the scanning electron microscope photograph form one data set from which the average domain size is calculated. The average domain size $\langle L \rangle$ for this picture is $6.5 \pm 2$ $\mu$m. The crystal growth direction is from top to bottom in the picture. (B) Close up within one crystal domain, revealing excellent crystalline order. The hexagonal arrangement is typical of a fcc 111 face.

below the boiling point. Multiple samples were grown at the same time in the oven to check the reproducibility.

For convenience, the height variable $z$ is defined as 10 mm minus the actual position on the substrate (Figure 1A). The position $z = 0$ corresponds to a height on the substrate of 10 mm. The position $z = 10$ mm corresponds to the bottom of the substrate because the crystal grows toward this position. The $z = 10$ mm position rests on the bottom of the beaker during the crystallization process.

**B. Thickness Measurement.** The thickness of each thin film opal was derived from the Fabry−Pérot fringes in the optical reflectivity spectra. The reflectivity spectra were measured with a setup similar to the one in ref 26 using a Fourier transform spectrometer (Biorad FTS6000). An objective with a small numerical aperture of 0.05 was used to focus the collimated beam onto the sample. Reflectivity spectra were measured at different spots along the $z$ axis of the substrate. An example of a reflectivity spectrum is shown in Figure 2.

The main features present in the spectrum are the Fabry−Pérot fringes and the reflectivity peak resulting from the first-order photonic stopband of the opal. The thickness $d$ of the sample can be calculated (in nm) from the spacing $\Delta\Omega$ of the fringes with

$$d = \frac{10^7}{2n_{\text{eff}}} \frac{\Delta m}{\Delta\Omega} \tag{1}$$

where $\Delta m$ is the difference in order between the different fringes, the fringe order, and $\Delta\Omega$ is the fringe spacing in $cm^{-1}$. We used all fringes on the red side of the stopband except the one closest to the stopband. The position of the fringe closest to the stopband is affected by photonic band bending. The effective refractive index $n_{\text{eff}}$ is taken to be the volume-averaged refractive index $n_{\text{eff}} = (1 - \phi)n_l + \phi n_h$, where $\phi$ is the volume fraction of silicon dioxide ($\phi = 0.74$ for fcc close-packed spheres), $n_l$ is the refractive index of the low-refractive-index material (in our case $n_l = 1$ for air), and $n_h$ is the refractive index of the high-refractive-index material ($1.465 \pm 0.004$ for silicon dioxide colloids[27]). A thickness of $d = 4.79$ $\mu$m can be derived from Figure 2, with $n_{\text{eff}} = 1.33$, $\Delta m = 2$, and $\Delta\Omega = 2083$ $cm^{-1}$. This specific point is shown in Figure 4B at $z = 5.5$ mm. The size of the error bars on the thickness measurements is conservatively estimated as 0.13 times the thickness. The number 0.13 is derived from statistics performed on sample spectra taken at random from the full set of measurements presented in this work. The distance between the

(24) Arriagada, F. J.; Osseo-Asare, K. *The Colloid Chemistry of Silica*; Bergna, H. E., Ed.; American Chemical Society: Washinghton, DC, 1994.
(25) Megens, M.; Wijnhoven, J. E. G. J.; Lagendijk, A.; Vos, W. L. *J. Opt. Soc. Am. B* **1999**, *16*, 1403.
(26) Thijssen, M. S.; Sprik, R.; Wijnhoven, J. E. G. J.; Megens, M.; Narayanan, T.; Lagendijk, L.; Vos, W. L. *Phys. Rev. Lett.* **1999**, *83*, 2730.
(27) Riese, D. O.; Vos, W. L.; Wegdam, G. H.; Poelwijk, F. J.; Abernathy, D. L.; Grübel, G. *Phys. Rev. E* **2000**, *61*, 1676.
(28) Koenderink, A. F.; Lagendijk, A.; Vos, W. L. *Phys. Rev. B* **2005**, *72*, 153102.

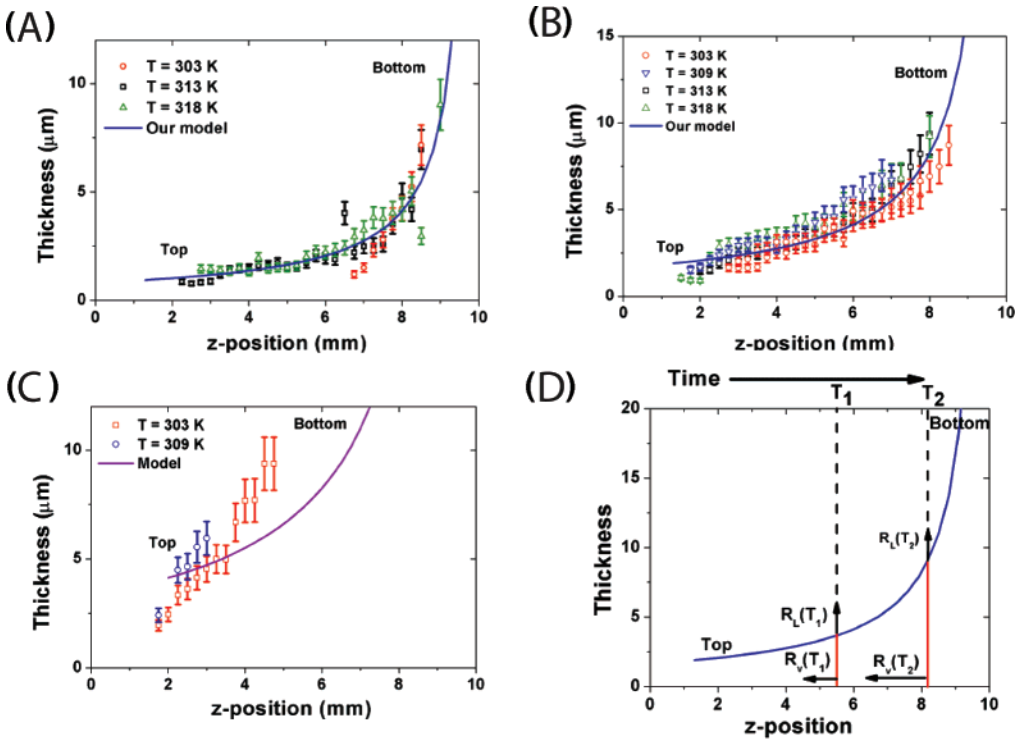


**Figure 4.** (A) Thickness of opals as a function of the *z* position on the sample. The opals were grown at different temperatures from dispersions with volume fractions of 0.05 (A), 0.10 (B), and 0.20% (C). The purple curve represents the model given by eq 2. Very good agreement between the theoretical curve and the measured data is observed. An increase in thickness toward the bottom of the sample is observed. (D) Schematic thickness as a function of the *z* position and time. The vertical lines in the graph indicate the thickness of the crystal at times $T_1$ and $T_2$. $R_v$ and $R_l$ are the vertical and lateral evaporation rates, respectively.

lattice planes can be derived from the stopband position with the use of Bragg's law, $d_{111} = \{\lambda_c\}/\{2n_{eff}\}$, with $\lambda_c$ being the position of the stopband. The distance between the lattice planes derived with Figure 2 is 197 $\mu$m.

No thickness data could be recorded if there were no fringes visible in the spectrum. This was in general the case near the bottom of the substrate. The reason is that the opals are so thick near the bottom that the coherence between the light reflected from the air−opal interface and from the opal−substrate interface is lost to extinction. The thickest measurable thickness was found to be about 10 $\mu$m.

**C. Domain Size Measurement.** The domain size ($L$) was measured with a scanning electron microscope (SEM), FEI XL30 SFEG. Figure 3A shows a scanning electron microscope photograph from the surface of an opal. The different crystal domains are irregularly shaped. The spheres are fcc-packed within one domain (Figure 3B). Adjacent crystal domains fit like pieces of a jigsaw puzzle, indicating that the cracks separating them were formed after the spheres ordered themselves in a crystal structure. The cracks are the result of stress formation during the drying of the crystal.

Each value of the average domain size is derived from a set of 10 values taken from an SEM picture like the one in Figure 3A. The size of the domain is systematically measured in both the horizontal and vertical directions with respect to the growth direction of the opal. The domain widths are drawn through the estimated center of mass of the domain. The first measurements of the set of 10 are always taken in the central domain of the SEM picture, followed by neighboring domains.

## III. Results and Discussion

**A. Visual Sample Appearance.** Figure 1B shows an optical microscope picture of a typical thin film opal photonic crystal. It shows the green color that results from the first-order Bragg diffraction. Furthermore, there are domains surrounded by visible cracks. In Figure 1B, it can be seen that the color of the sample is not homogeneous. The green color at the top of the thin film crystal is lighter than the green color at the bottom of the sample. A more careful look at the optical microscope picture also reveals large domains at the bottom of the sample. The domains become smaller toward the top and become irresolvable by the optical microscope. The inhomogeneity of the sample is already apparent from the optical microscope picture. In the next sections, the inhomogeneity will be quantified.

**B. Thickness of the Opal as a Function of Height.** Figure 4A shows the thickness of opals grown from a dispersion with a volume fraction of $\Phi_i = 0.05\%$ v/v. The opals starts to grow at the initial dispersion level, $z = 2$ mm. The Figure shows that the opals become thicker with increasing $z$, that is, near the bottom of the substrate. The thickness profiles that we measured are found to be independent of temperature. We observe that the thickness of each sample is not homogeneously distributed but is strongly dependent on the position on the sample. We therefore recommend that the thickness be measured for several positions on a sample, as an improvement of the commonly performed characterization of only one thickness measurement.

We know the initial volume fraction of the dispersion $\Phi_i$, and we may assume that the number of crystallized spheres is negligible with respect to the number left in the dispersion. In this case, the volume fraction of spheres in solution is doubled if half of the solvent has evaporated. We have assumed a linear relation between the thickness of the crystal and the volume fraction, as proposed in ref 5. Therefore, the height-dependent thickness profile is taken to be

$$d(z) = d_0 \frac{10 - z_0}{10 - z} \frac{\Phi_i}{\Phi_0} \qquad (2)$$

where $d$ is the thickness of the crystal, $d_0$ is the thickness of the crystal at the starting position of crystal growth, and $z_0$ is the $z$

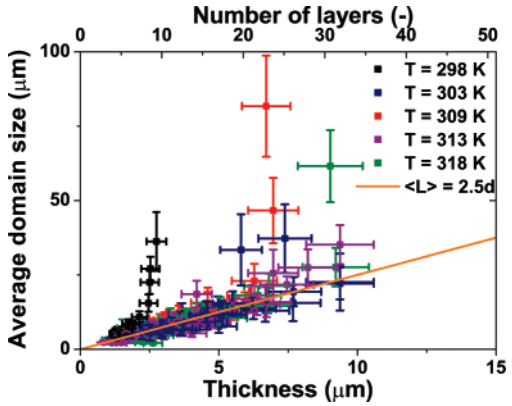


**Figure 5.** Average domain size of opals synthesized at different temperatures and volume fractions as a function of the thickness of the opal for a total 300 data points. The average domain of an opal is 2.5 times wider than it is thick. All data points from samples grown at the same temperature are the same color.

position on the substrate where crystallization started. In the case of Figure 4A, $z_0 = 2.5$ mm and $d_0 = 1.1$ $\mu$m. The resulting curve is plotted in Figure 4A and is seen to overlap the data points excellently at all temperatures.

Figure 4B shows the measured thickness for samples grown with an initial volume fraction of $\Phi_i = 0.10\%$. We see that the thickness profiles are strikingly independent of temperature. The data shows the same trend as the data from Figure 4A: an increase in thickness toward the bottom of the substrate is observed, and the thickness of the opal is not constant. The model curve is the curve from Figure 4A scaled with the ratio of the initial bulk volume fractions $\Phi_i$ as given by eq 2. The data shows very good agreement with the curve from eq 2, with only a slight deviation for small and large thicknesses.

Figure 4C shows the thickness measurements for two samples grown from dispersions with an initial volume fraction of $\Phi_i = 0.20\%$ at two different temperatures. The $z$ position of the 303 K data was scaled with the initial volume with respect to the 309 K curve because the initial dispersion volume was less. Again the thickness increases with the $z$ position and is independent of temperature, and no extra parameters are used. Only the ratio of the initial volume fraction is taken to be the value of $\Phi_i = 0.20\%$. With increasing $z$, the measured thickness becomes larger than the thickness predicted by eq 2.

Equation 2 holds very well for volume fractions of $\Phi_i = 0.05\%$ (Figure 4A) and for 0.10% (Figure 4B). The validity of eq 2 suggests that the volume fraction in either the dispersion or in the meniscus is homogeneous. The increase in volume fraction near the meniscus by the collection of spheres at the meniscus is canceled by the concentration-driven diffusion of spheres from the meniscus to the bulk. The curve from eq 2 agrees for $z$ between 2 and 4 mm with the data for a high initial volume fraction of $\Phi_i = 0.20\%$ (Figure 4C). For larger $z$, the measured thickness is larger than predicted with eq 2. This observation suggests that there is a larger flow of spheres to the substrate in the case of higher concentration than in the case of lower concentration. The larger flow might be caused by an accumulation of spheres near the meniscus at the air/solvent interface. The reason could be the changed equilibrium of the dispersion dynamics at increased particle density.

**C. Drying and Domain Formation.** Figure 5 shows the domain size as a function of thickness for samples grown at five different temperatures ranging from 298 to 318 K. Figure 5 shows that the average domain size increases linearly with thickness. The total number of data points shown is 300, of which only 9 deviate from the linear trend depicted by the orange line. The ratio between the average domain size and the thickness of the thin film opal is 2.5. This means that on average the opal domains formed on the substrate are 2.5 times wider than thick. We propose that the origin of the linear relation between the average domain size and the thickness might lie in the viscous behavior of the opal layer during the drying process. Forces work at the air−wet opal interface during the drying process and are distributed linearly through the wet layer. If this is the case, then the force per unit thickness is inversely proportional to the thickness. If we furthermore assume that there is some force proportional to the perimeter of the domain preventing domain formation, then it would follow that the domain size increases with thickness in the case of a viscous layer. The consequences for optical measurements are discussed in section III E.

The domain size to thickness ratio of 2.5 can be compared to values in the literature. The linear relation that we found agrees with previously found results for completely different colloid systems.[18] A ratio between 3.75 and 6.25 was found for layers of alumina/water slurry.[18] The higher ratio was obtained by using a smoother substrate to reduce the friction between the opal layer and the substrate. Reducing the number of impurities also increases the ratio. We estimated a ratio of 1.5 from data on the directional drying of silica particles of up to 10 nm in radius.[16] Our results show that the linear relation between domain size and thickness also holds if colloidal spheres crystallize while the dispersion dries. Finally, our observation that crack formation occurs at all thicknesses, including those smaller than 10 $\mu$m, contradicts the results in ref 22 for currently unknown reasons.

Figure 6A shows domains near the top of the substrate at a height of $z = 5.5$ mm. The domains at these positions are very irregularly shaped. The crystals on both sides of the cracks have the same crystal orientation, and the domains fit each other like pieces of a jigsaw puzzle despite their irregular shape. This appearance was observed earlier.[5] Figure 6B shows a scanning electron microscope photograph of the crystal closer to the bottom at a height of $z = 8.25$ mm. It can be seen that the domains are rectangularly shaped and surrounded with large cracks parallel to the growth direction, which is from top to bottom in the Figure.

The difference in domain shape has been investigated by Shorlin et al. and indicates a different drying mechanism: irregularly shaped domains in drying films are found in isotropic drying, whereas the rectangularly shaped domains accompanied by large vertical cracks are a signature of directional drying.[18] This suggests that directional drying is dominant at the bottom of the samples where we find the larger rectangularly shaped domains. However, the crystal dries isotropically at the top of the sample. This can be understood if we also take the thickness of the samples into account as shown in Figure 4D: The crystal has two perpendicular interfaces with the air surrounding it. The first one is horizontal and perpendicular to the growth direction and is indicated in Figure 4D with vertical lines. This interface becomes larger when the crystal becomes thicker. The vertical line in Figure 4D at time $T_1$ and that at later time $T_2$ illustrate this feature. The vertical evaporation rate $R_v$ increases with time because of the increase in the vertical interface. The second interface is a vertical surface parallel to the growth direction and the substrate. This surface remains constant throughout the drying process and moves downward; therefore, the lateral evaporation rate $R_l$ is constant in time, as indicated by equal lengths for $R_2$ at time $T_1$ and $R_2$ at time $T_2$ in Figure 4D.

If we consider a piece of wet crystal at the top ($T_1$), then Figure 4D shows that the ratio between the horizontal and vertical surface is smaller than in the case of a piece of wet crystal at the bottom

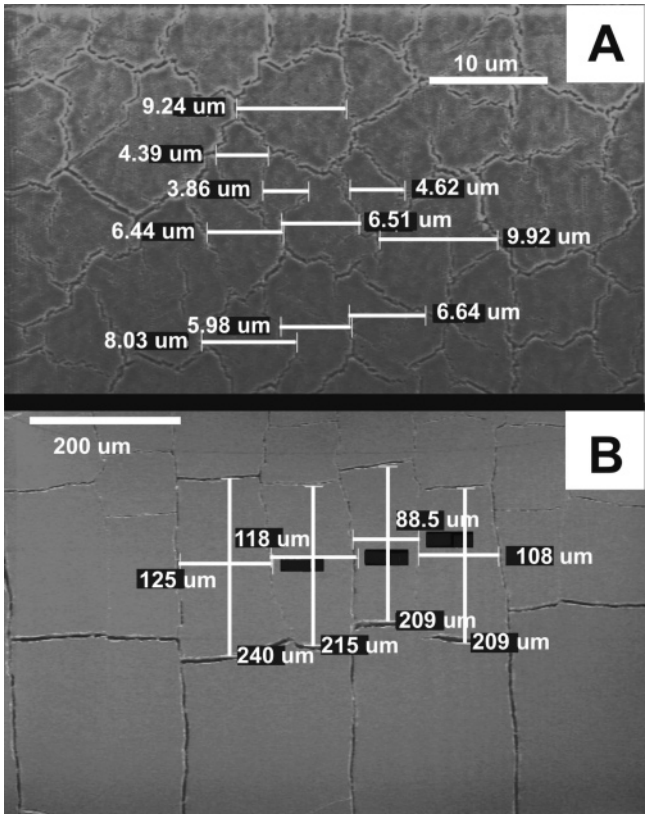


**Figure 6.** (A) Scanning electron microscope photograph of an opal at a *z* position of 5.5 mm. The crystal domains can clearly be distinguished. The domains are shaped irregularly near the top of the crystal, which indicates isotropic drying. The growth direction of the crystal is from top to bottom. (B) Scanning electron microscope photograph of an opal at a *z* position of 8.25 mm. The crystal domains can clearly be distinguished. The domains are shaped rectangularly near the bottom of the crystal, which indicates directional drying. The growth direction of the crystal is from top to bottom.

of the substrate ($T_2$). Therefore, the ratio of $R_v$ to $R_l$ is smaller at the top of the sample than at the bottom of the sample. This means that at the bottom of the sample the total evaporation speed is dominated by the vertical evaporation rate $R_v$. The crystal dries directionally in this area. At the top of the sample, the lateral evaporation rate $R_l$ is larger, which results in isotropic drying at the top of the sample. Furthermore, the sum of the interfacing surface between the air and wet crystal increases toward the bottom of the substrate, which means that the evaporation speed is faster at the bottom of the crystal, thus giving the spheres less time to organize themselves. This effect becomes even stronger because there are more spheres that need to be ordered.

We conclude that the crystal dries isotropically at the top of the sample whereas it dries directional at the bottom of the sample. Furthermore, we have shown that drying phenomena known from disordered structures[16,18,22] also apply to ordered structures. This fact gives us the possibility to conclude that a smoother substrate will lead to crystals with larger domains than the ones that we have presented in this article.

**D. Domain Size of the Opal as a Function of Height.** Figure 7 shows the average domain size as a function of the *z* position for three different samples grown at 309 K. The initial volume fraction of the three samples was varied. Figure 7 shows an increase in domain size with *z* position. The largest domains with sizes up to 150 $\mu$m can be found at the bottom of the sample. The sample grown at an initial volume fraction of $\Phi_i = 0.40\%$ was damaged by the tension built up during drying so that no

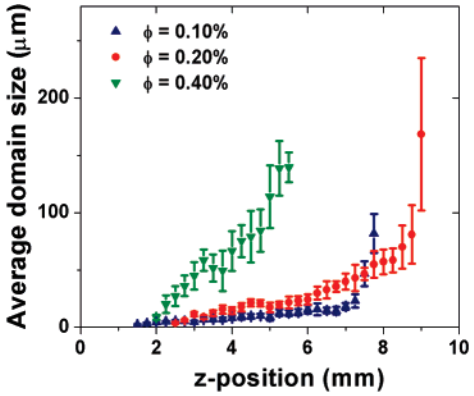


**Figure 7.** Average domain size of opals grown at different volume fractions and at $T = 309$ K as a function of the *z* position on the sample. An increase in average domain size toward the bottom of the substrate is observed for all three volume fractions.

more crystal domains were present on the substrate above $z = 6$ mm. A comparison with other samples showed no effect of temperature on the domain size profile. We again observe that the size of the different domains on each sample is inhomogeneous: the size of the domain is strongly dependent on the position on the sample. Therefore, we recommend that the position is also mentioned when data on domain sizes is shown.

**E. Consequences for Photonic Crystals.** For photonic crystals, domains are required that are as large as possible combined with a controlled thickness. Our results show that the possible combinations are limited. Because the ratio of the thickness and domain size is fixed, this means that the density of grain boundaries is related to the opal thickness. The grain boundaries increase the unwanted extinction of light because the boundaries contribute to the scattering of light out of the coherent beam. The extinction due to scattering from grain boundaries is therefore fixed for each thickness. This means that there is an upper limit to the reflectivity measured in the stopgaps if the focus of the light beam is larger than a crystal domain. This in turn means that there is a lower limit to the range of thicknesses for which the scattering from grain boundaries can be reduced to zero, given a certain focus size of the light beam.

The quality of the opal is likely to be influenced by the drying regime. If the isotropic drying process yields better crystals, then there will be a upper limit to the thickness of a good crystal, according to Figure 4D. If directional drying yields better crystals, then there will be a lower limit to the thickness of a good crystal. To be able to give a prediction about the quality of opals formed in either of the two drying regimes, we assume the following mechanism: the spheres self-assemble in close-packed order at the wet crystal−air interfaces, and the spheres below the upper layer organize themselves to form another closed-pack layer. The second step was discussed by Norris et al.[11] The assumed mechanism suggests that the quality of the crystal in the direction perpendicular to the wet crystal−air interface is higher than in another direction because the spheres order themselves according to the first crystal layer that formed at the wet crystal−air interface. Therefore, we predict that the quality will be better for films formed in the isotropic drying regime for measurements on the ⟨111⟩ planes of the crystal, which lie parallel to the substrate.

## IV. Conclusions

We have grown thin film opals via vertically controlled drying by systematically varying the temperature and initial volume fraction. We have measured the thickness of the resulting opals. The thickness increases with the *z* position, independent of

temperature. The thickness profile agrees with a simple model for thickness variation with colloid density.

We have investigated the lateral size of crystal domains of the grown opals. We found that the domain size increases with $z$ position. We found a surprisingly linear relation between the lateral domain size and the crystal thickness. The ratio between the domain size and the thickness is found to be 2.5. It is interesting to see that the drying behavior is similar to the behavior of drying slurries of polydisperse particles. We compared the obtained domain size-to-thickness ratio with the literature and concluded that a smoother substrate will increase the ratio yielding larger crystal domains. We identified two sample regions with different drying behavior. We proposed a qualitative explanation of the drying mechanism of self-assembled photonic crystals grown with vertically controlled drying.

We conclude that the structural properties of a thin film opal photonic crystal are inhomogeneous. Therefore, we recommend that the position at which the characteristics are measured is given as well. The thickness profile is easily determined with the thickness at a certain position by using the functional relation presented.

Finally, our data shows that the lateral domain size increases with increasing thickness of the crystal. Therefore, in photonic applications the grain-boundary-induced scattering of light is reduced for thick crystals and prominent for thin crystals.

**Acknowledgment.** We thank Bart Husken for optical microscopy and Léon Woldering, Daan Frenkel, and David Norris for stimulating discussions. This research was supported by NanoNed, a nanotechnology programme of the Dutch Ministry of Economic Affairs, and by a VICI fellowship from the Nederlandse Organisatie voor Wetenschappelijk Onderzoek (NWO) to W.L.V. This work is also part of the research programme of the Stichting voor Fundamenteel Onderzoek der Materie (FOM), which is financially supported by the NWO.

LA800137E